Electronic Structure of Fullerene Acceptors in Organic Bulk-Heterojunctions: A Combined EPR and DFT Study

Kristy L. Mardis,[†, ‡, *] *Jeremy N. Webb,*[†] *Tarita Holloway,*[†] *Jens Niklas,*[‡] *Oleg G. Poluektov*[‡, *]

† Department of Chemistry and Physics, Chicago State University, Chicago, Illinois 60628, USA

‡Chemical Sciences and Engineering Division, Argonne National Laboratory, Argonne, Illinois 60439, USA

AUTHOR INFORMATION

Corresponding Author

*Kristy L. Mardis (kmardis@csu.edu; Phone: (773) 995-2171); Oleg G. Poluektov (oleg@anl.gov; Phone: (630) 252-3546)

ABSTRACT

Organic photovoltaic (OPV) devices are a promising alternative energy source. Attempts to improve their performance have focused on the optimization of electron-donating polymers, while electron-accepting fullerenes have received less attention. Here, we report an electronic structure study of the widely used soluble fullerene derivatives $PC_{61}BM$ and $PC_{71}BM$ in their singly reduced state, that are generated in the polymer:fullerene blends upon light-induced charge separation. Density Functional Theory (DFT) calculations characterize the electronic structures of the fullerene anions through spin density distributions and magnetic resonance parameters. The good agreement of the calculated magnetic resonance parameters with those determined experimentally by advanced EPR allows the validation of the DFT calculations. Thus, for the first time the complete set of magnetic resonance parameters including directions of the main g-tensors axis were determined. For both molecules, no spin density is present on the PCBM side chain and the axis of the largest g-value lies along the PCBM molecular axis. While the spin density distribution is largely uniform for $PC_{61}BM$, it is not evenly distributed for $PC_{71}BM$.

TOC GRAPHICS

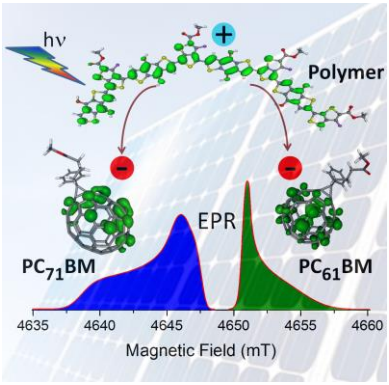

KEYWORDS

$PC_{61}BM$, $PC_{71}BM$, Polaron, Radical Anion, Electron Transfer, Spin Density, g-tensor.

Global energy demands are predicted to increase by 35% in the next 25 years.[1] For various reasons, this demand cannot continue to be met by relying solely on fossil fuels.[2] The best way to overcome the global dependence on fossil fuels is to switch to renewable energy sources such as sunlight, wind, water, biomass, and geothermal.[2-3] Comparative analysis shows that potentially the most promising, clean and sustainable resource is solar energy.[4-6] There are number of ways to utilize and harvest solar energy. The most common are known as solar-to-fuel and solar-to-electricity approaches.[6-7] In the former case, solar energy is transformed and stored in the energy of chemical bonds of the fuel, while in the latter case solar energy is stored as electrical potential of separated charges by utilizing photovoltaic (PV) solar cells. Currently, industrial energy production almost exclusively uses silicon based PV devices. The organic PVs (OPV) and hybrid PVs, such as recently emerging perovskite PVs, are fields of extensive research and development.[8-11] OPV devices are already in use in applications which have special demands like light weight and transportability, where those devices have distinct advantages over conventional PV devices.[12]

The initial discovery of charge transfer in polymer-fullerene systems, and thus their possibilities as organic photovoltaic cell materials was made in 1992.[13] While at first device efficiencies were very low, they are now generally between 8-9% with a recent report of 10.7%.[14-15] Upon light excitation, the neutral excitons break down into two spin-carrying charged counterparts, the positive and negative polaron on the polymer and the fullerene, respectively.[8, 16] Using the chemical/molecular terms instead of the solid state physics terms, light irradiation creates excited singlet states which subsequently decay via charge transfer to radical cations and radical anions. Since the organic bulk-heterojunctions (BHJ) under investigation lack many of

the characteristics of distinctive semiconductors, but have the characteristics of molecular systems, the use of the chemical terms seems more appropriate and is used in the following.

Much recent research has focused on the improvement of the polymer-donor materials resulting in the design of many novel low band gap polymers.[8, 17-18] Most of the novel polymers and their corresponding radical cations have been well characterized and computational approaches have been used to model experimental data and their electronic structure.[8, 16, 19] However, other than the invention of the soluble derivatives of C_{60} and C_{70} (termed $PC_{61}BM$ and $PC_{71}BM$, respectively),[20-21] changes to the electron acceptors have not resulted in significant improvements to the efficiencies. Furthermore, the computational treatment of the fullerenes remains a challenge due to their complex electronic structure with large numbers of degenerate, or close to degenerate states.

To reveal the electronic structures of the light-induced anion radicals localized on the fullerene derivatives $PC_{61}BM$ and $PC_{71}BM$, in the polymer-fullerene OPV active blends, we have used advanced EPR spectroscopy combined with Density Functional Theory (DFT) calculations. These two fullerene derivatives are the most widely used ones in OPV materials (Scheme 1).

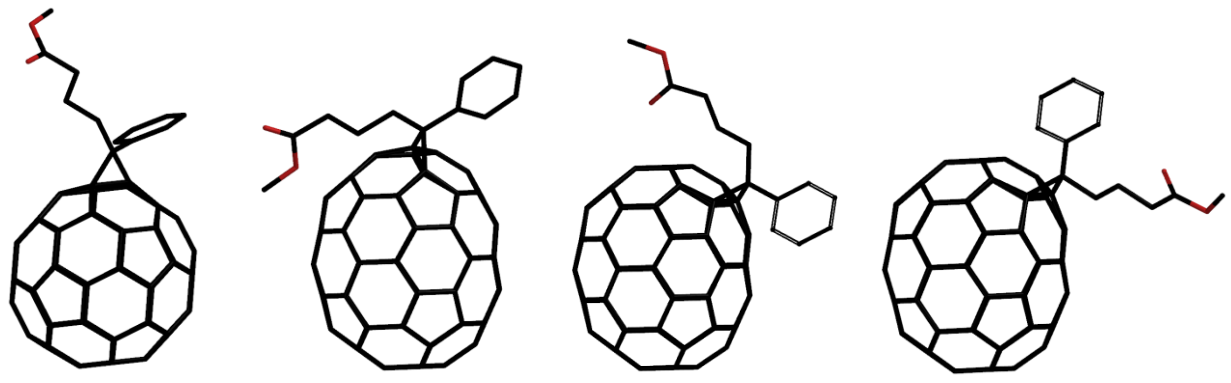

$PC_{61}BM$ α-$PC_{71}BM$ β_1-$PC_{71}BM$ β_2-$PC_{71}BM$

Scheme 1. Structures of the C_{60}- and C_{70}-derivatives: [6,6]-phenyl C_{61} butyric acid methyl ester ($PC_{61}BM$) and isomers of [6,6]-phenyl C_{71} butyric acid methyl esters ($PC_{71}BM$).[20-21] The three $PC_{71}BM$ isomers are shown in the same orientation to aid in the visualization of the PCBM side chain location. Red color indicates the position of oxygen atoms.

The radical anions of the fullerene derivatives were created at low temperature by *in situ* illumination of corresponding BHJ fullerene:polymer blends in the resonator of the EPR spectrometer. P3HT was used as the polymer component in the blends, since it has been used in many previous studies and is well characterized. EPR spectra, which are the "spin signature" of the radical's electronic state, were recorded by conventional X-band EPR and by high frequency D-band EPR spectroscopy. While conventional X-band (9-10 GHz) EPR spectroscopy allows to largely separate the signals of anion and cation radicals on $PC_{61}BM$ and P3HT, their g-tensors are not fully resolved (Figure 1, left panel). In the case of the $PC_{71}BM$:P3HT blend the EPR signals of negative and positive radicals are strongly overlapped at X-band. These problems were addressed by using high frequency D-band (130 GHz), which has 14 times greater g-tensor resolution compared to conventional X-band (Figure 1, right panel). Computer simulation of the spectra yielded magnetic resonance parameters as shown in Table 1. The D-band EPR spectra of both fullerene radical anions demonstrate almost axial symmetry of the g-tensors with very broad parallel components. However, there is a striking difference between the EPR "spin signatures" of anion radicals (negative polarons) in $PC_{61}BM$ and $PC_{71}BM$, namely, the unexpected shift of the g-values of the $PC_{71}BM$ anion compared to the $PC_{61}BM$ anion. In particular, as shown in

Figure 1 and Table 1, all three $PC_{61}BM$ g-values are less than the free electron g-value, $g_e \approx 2.0023$, similar to that of shallow-trapped electrons in semiconducting materials,[22-23] while the $PC_{71}BM$ g-values are around or greater than g_e, which is typical for shallow-trapped donors in semiconductors [24] or pure organic radicals.[25-27]

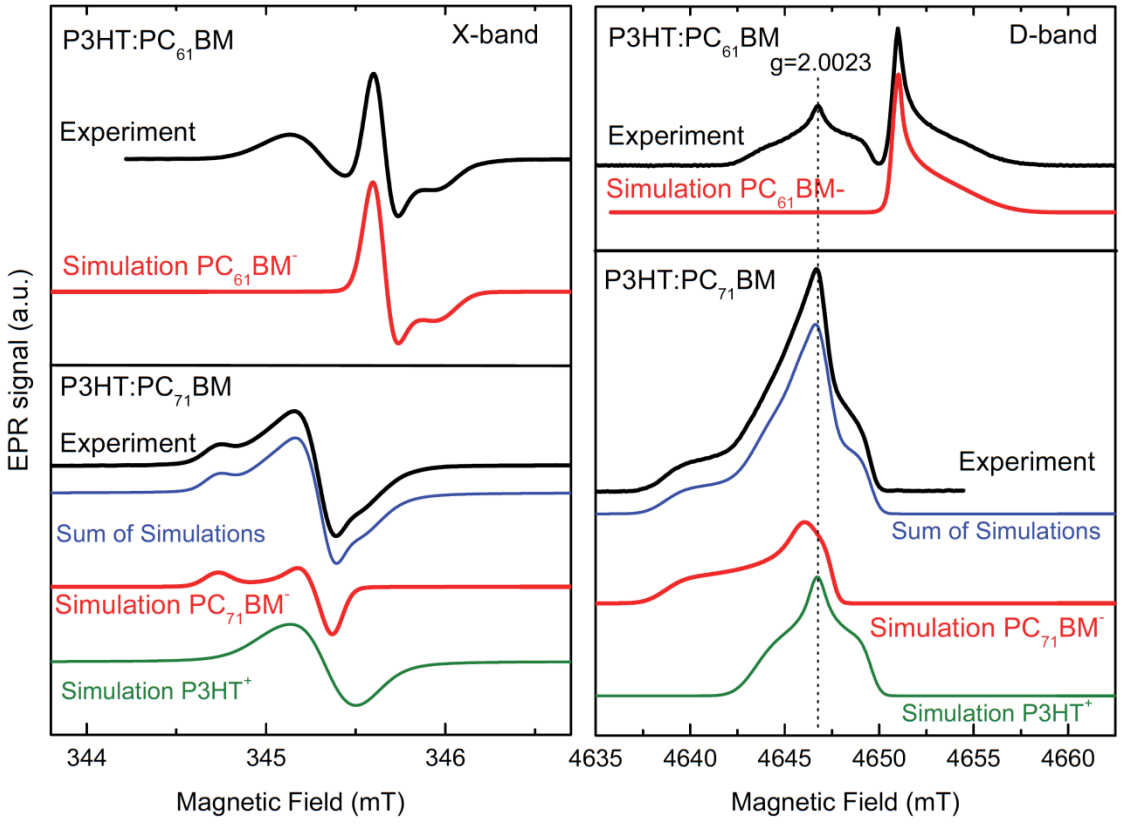

Figure 1. EPR spectra of $PC_{61}BM$ and $PC_{71}BM$ radical anions at X-band (9-10 GHz) and D-band (130 GHz). The fullerene radical anions have been created by light-induced electron transfer in the BHJ blends (with P3HT) at low temperature. Continuous wave (CW) X-band EPR spectra were recorded as first derivatives of the absorption, while pulsed D-band EPR spectra were recorded as absorption. Experimental traces are in black, computer simulations of the fullerene radical anions in red, computer simulations of P3HT radical cation in green, sum of computer simulations in blue. Simulation parameters are summarized in Table 1.

Although the difference in g-values between $PC_{61}BM$ and $PC_{71}BM$ radical anions has been reported before,[28-31] a satisfactory explanation for this striking deviation has yet to be presented. For fullerenes in general, these shifts have been tentatively attributed to the spin-orbit interaction on a distorted fullerene cage,[13] to the static Jahn-Teller effect,[32-33] or to differences in the Jahn-Teller dynamics for C_{60} and C_{70} molecules.[32] Moreover it is not clear why, in spite of the high symmetry of the fullerene molecules, the g-tensor of $PC_{61}BM$ as well as $PC_{71}BM$ anion is anisotropic. Currently, there is no unified theory that can explain g-tensors of both C_{60}^- and C_{70}^- radicals. To address these questions we use DFT modeling to calculate the electronic structure and combine this with experimental EPR data to verify the validity of the theoretical approach. We have recently shown that this type of approach can be successfully applied to OPV materials.[31, 34-36]

As shown in Table 1, there is a good agreement between experimental and calculated values of the g-tensor for the $PC_{61}BM$ anion. Note, that we listed the g-values as $g_3>g_2>g_1$ where g_1, g_2, and g_3 are the principal axis components of the g-tensor. The values for g_2 and g_3 are nearly identical while g_1 is much smaller. This is in contrast to $PC_{71}BM$, where both calculated and

experimental values of g_1 and g_2 are similar in magnitude and the largest g-value (g_3) stands out. Evaluating the precise agreement between experimental and calculated values for the $PC_{71}BM$ anion is complicated as the symmetry of C_{70} allows three possible isomers when the PCBM side chain is attached (Scheme 1).[21] While it is generally accepted that the synthesized molecule exists in a roughly 85/15 split between the α and two β isomers, the precise isomer ratio may depend upon the particular synthetic pathway and purification procedure. According to our DFT calculations, all isomers have slightly different g-values (Table 1), and the difference in resonance field is comparable in magnitude to the line broadening in D-band EPR spectra. This makes direct comparison of theoretical and experimental data less straightforward. Weighted average values of the calculated g-tensor components (shown in Table 1) demonstrate a reasonable agreement with the experiment. For $PC_{61}BM$ and α-$PC_{71}BM$ the calculated g-values were essentially unchanged by the choice of various basis sets for both the optimization and the EPR parameter calculation, while for the two β-isomers of $PC_{71}BM$ a very weak dependence on the basis set was found (Supporting Information Tables S1-S2).

Table 1. The principal values of the g-tensors of the fullerenes radical anions as determined experimentally in frozen toluene solution of P3HT:fullerene blends and calculated using the EPRII basis set and B3LYP functional for the structures optimized at the 6-31G+(d)|B3LYP level (see below for details). The relative error of the experimental g-values is ± 0.0001; due to large g-strain effects, the error is ± 0.0003 for g_1 of $PC_{61}BM$ and g_3 of $PC_{71}BM$. Numbering of the g-values follows the scheme employed by the ORCA program package, $g_3>g_2>g_1$.

	$PC_{61}BM^{\bullet-}$	$PC_{61}BM^{\bullet-}$	$\alpha\ PC_{71}BM^{\bullet-}$	$\beta_1PC_{71}BM^{\bullet-}$	$\beta_2PC_{71}BM^{\bullet-}$	$PC_{71}BM^{\bullet-}$	$PC_{71}BM^{\bullet-}$
g	Calculated	Experimental	Calculated	Calculated	Calculated	Avg*	Experimental
$\mathbf{g_3}$	2.0009	2.0006	2.0054	2.0048	2.0047	2.0053	2.0060
$\mathbf{g_2}$	2.0008	2.0005	2.0035	2.0029	2.0029	2.0034	2.0028
$\mathbf{g_1}$	1.9995	1.9985	2.0026	2.0019	2.0017	2.0025	2.0021

*Calculated values are averaged 85% α; 15% β_1 and β_2. These values follow the distribution of isomers reported in ref. [21].

Note that the calculations somewhat underestimate the g-tensor anisotropy (g_3-g_1 difference) for $PC_{71}BM$ although agreement is still good. Previously we reported a solution dependent shift of the g_3 as well as strain effect on the g_3-component of the same order of magnitude, < 0.001.[31] For organic radicals, a shift of this magnitude may be due to environmental effects, when a large fraction of spin density is localized on atoms with large spin-orbit coupling, such as oxygen (or nitrogen). In these cases, the solvent is very often engaged in direct hydrogen bonding with the oxygen (or nitrogen) atom.[37-39] However, as shown below, the fullerenes under study have two oxygen atoms with large spin orbit coupling constants but insignificant spin density on these oxygen atoms. Moreover, the unpaired electron is strongly delocalized over the fullerene cage, which makes an effect of specific interaction negligible. We observed that g-strain depends not only upon the solvent but also upon sample preparation: freezing and annealing protocol, i.e. nonspecific interaction with an environment. Based on these data we tentatively attribute g-strain and g-shift of the parallel components in $PC_{61}BM$ (g_1) and $PC_{71}BM$ (g_3) anions to the mechanical deformation of the fullerene cages by the solid environment which exerts pressure on the fullerene molecule in films or frozen solutions.

In order to better understand and visualize the differences in the electronic structures between $PC_{61}BM$ and $PC_{71}BM$ radical anions we used DFT to calculate the spin density distribution

(Figure 2). For all four fullerenes, virtually no spin density is found on the side chain; for $PC_{61}BM$ less than 0.2% of the unpaired spin density is present on the side chain; for α–$PC_{71}BM$, less than 0.3% on the side chain. The calculated electron hyperfine coupling with the side chain protons is less than 0.5 MHz, which is similar to the pure dipole electron-nuclear interactions with matrix (distant) protons and in excellent agreement with the ENDOR data reported for the $PC_{61}BM$ radical anion.[31]

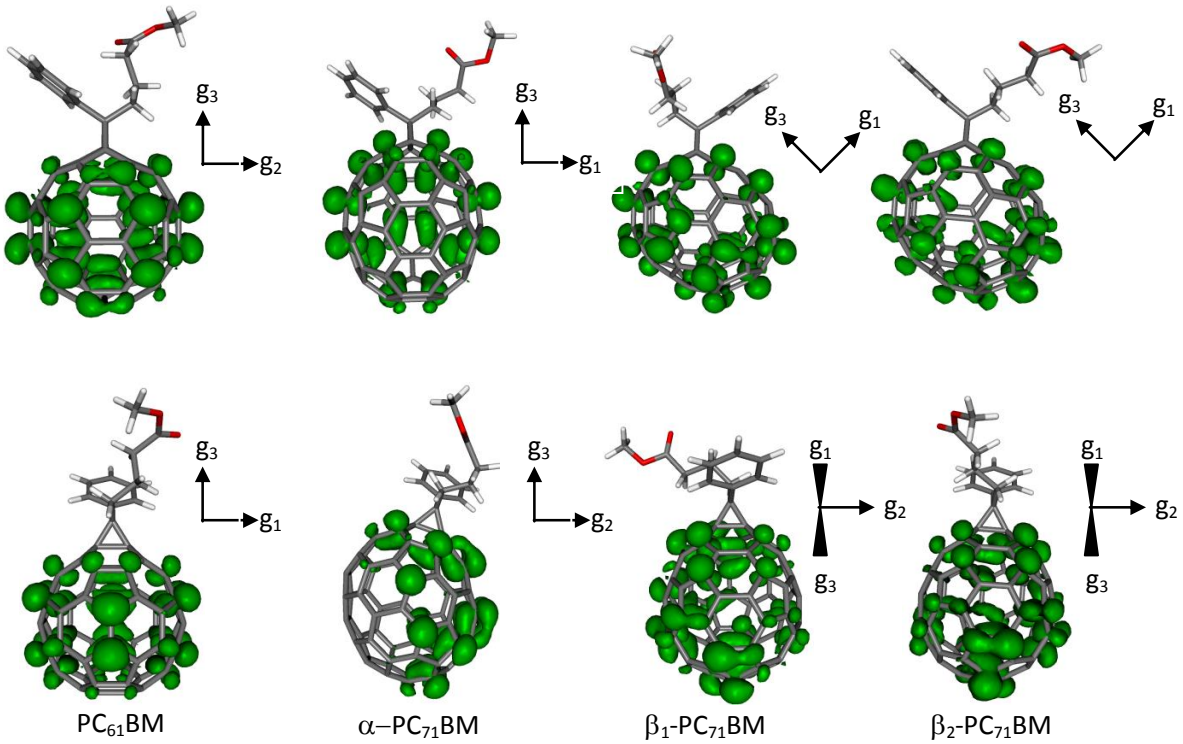

Figure 2. Spin density iso-surface plots (B3LYP|EPRII) of the optimized lowest energy conformation (B3LYP|6-31G+(d)) for each of the fullerene radical anions studied. All iso-surfaces are shown at a contour level of 0.001 e/a_0^3. The second row shows orientations rotated

90 degrees with respect to the first row. Arrows show the orientation of the principal axes of the g-tensors.

While the g-tensor axes shown in Figure 2 vary between $PC_{61}BM$ and $PC_{71}BM$ radical anions, the axis of the largest g-value (g_3) is always aligned with the principal axis of the fullerene cage: this is the elongation axis for $PC_{71}BM$ and the axis connecting the center of the fullerene and cyclopropyl ring of side chain for $PC_{61}BM$. This results in alignment of the principal molecular axis and the largest g-tensor axis (g_3) for $PC_{61}BM$ and the α-isomer of $PC_{71}BM$. In contrast, for the two β-isomers of $PC_{71}BM$, where the side chain is bound to a less polar bond[21, 40] off center of the long axis of the C_{70} cage (see Scheme 1), the largest g-value remains aligned with the fullerene elongation axis, and is skewed with respect to the side chain. Note, that for $PC_{61}BM$ the g_1 component and for all three $PC_{71}BM$ isomers the g_2 components are in the plane of the cyclopropyl ring. This suggests that even though the side chain carries essentially no spin density, its addition and resulting symmetry breaking of the fullerene cage contributes to the g-tensor anisotropy.

An important finding is that the spin localization pattern on the fullerene cage exhibits noticeable differences between the $PC_{61}BM$ and $PC_{71}BM$ radical anions. For $PC_{61}BM$ the spin density is delocalized broadly in a kind of "belt" around the entire molecule, while for the $PC_{71}BM$ molecules, the spin density is localized on one side of the molecule (Figure 2); this is most visible for the α-isomer. The difference in spin density delocalization is reproduced in calculations with different basis sets (SI Table S2). While it has been suggested that the B3LYP functional is non-ideal for the calculation of spin properties due to errors in its treatment of

correlation effects,[41] the non-symmetric delocalization in spin density persists for all functionals used in our calculations with different inclusion of correlation (SI Table S3). Furthermore, the agreement between g-values calculated using different functionals and basis sets and experimental g-values supports our spin density calculations. Despite the different distributions of spin density, both $PC_{61}BM$ and $PC_{71}BM$ have approximately the same percentage of carbons with very small and very large spin populations (SI Tables S6-S7 and Figure S2). Therefore, the primary difference between $PC_{61}BM$ and $PC_{71}BM$ radical anions is the spin density delocalization pattern. We propose that the observed difference in delocalization pattern is responsible for the shift of the g-values of $PC_{71}BM$ compared to $PC_{61}BM$.

To summarize, we have carried out a comprehensive EPR and DFT study of the characteristic EPR signals of the fullerene radical anions in polymer-fullerene BHJ blends. EPR spectroscopy reveals a remarkable difference in the g-values of anion radicals of $PC_{61}BM$ compared to $PC_{71}BM$ in BHJ blends. This difference was correctly reproduced by DFT calculations which demonstrate that almost no spin density is present on the PCBM side chain. Furthermore, the three $PC_{71}BM$ structures have spin density localization patterns that are not symmetric with respect to the molecule, while the $PC_{61}BM$ spin density contours uniformly ring the entire molecule. We propose that this difference in spin density pattern is accountable for the different shifts of the g-values of $PC_{61}BM$ and $PC_{71}BM$ with respect to the free electron g-value, g_e. We also tentatively assign the pronounced g-strain effect in the parallel components of the fullerene radical anion g-tensors to the mechanical interactions of the flexible fullerene cage with the heterogeneous environment of BHJ. The largest g-tensor axis lies along the long axis of the fullerene cage for $PC_{71}BM$ irrespective of the location of the side chain, and along the axis connecting center of the fullerene and cyclopropyl ring of side chain for $PC_{61}BM$. This work

clearly demonstrates that advanced EPR spectroscopy in combination with DFT is an extremely powerful approach for investigation of the electronic structure of the charge separated states in organic photovoltaic materials.

EPR spectroscopy.

EPR samples of P3HT:fullerene blends were prepared as previously described.[31]

Continuous wave (cw) X-band (9-10 GHz) EPR experiments were carried out with a Bruker ELEXSYS E580 EPR spectrometer (Bruker Biospin, Rheinstetten, Germany), equipped with a Flexline dielectric ring resonator and a helium gas-flow cryostat (CF935, Oxford Instruments, UK). Light excitation was done directly in the resonator with 532 nm Laser light (Nd:YAG Laser with OPO, model Vibrant from Opotek) or a 300 W Xenon lamp (LX 300F from Atlas Specialty Lighting). When using the lamp, a water filter (20 cm pathlength) was used to avoid unwanted heating of the sample. In addition, a KG3 short pass filter (Schott) removed residual IR irradiation. In both setups (Laser and lamp), a GG400 long pass filter (Schott) was used to remove UV light. Typical incident light intensities at the sample were around 2 W for the lamp and 40 mW for the Laser. High frequency (HF) EPR measurements were performed on a home-built D-band (130 GHz) spectrometer equipped with a single mode TE_{011} cylindrical cavity.[42-43] EPR spectra of the samples were recorded in pulse mode in order to remove the microwave phase distortion due to fast-passage effects at low temperatures. Light excitation was done directly in the cavity of the spectrometer with 532 nm Laser light through an optical fiber (Nd:YAG Laser, INDI, Newport). Data processing was done using Xepr (Bruker BioSpin,

Rheinstetten) and MatlabTM 7.11.1 (MathWorks, Natick) environment. Simulations of the EPR spectra were performed using the EasySpin software package (version 4.0.0).[44]

Density Functional Theory (DFT) Calculations.

Initial fullerene structures were constructed from available C_{60}[45] and C_{70}[46] model compounds and pre-built and optimized PCBM fragments. The geometry optimizations were carried out using density functional theory (DFT) and the B3LYP functional[47-50] using, successively, the 3-21G, 6-31G, and the 6-31G+(d) basis set, as implemented in PQSMol.[51] Frequency calculations were performed on all optimized structures to ensure stable minima were obtained. The spectroscopic parameters were obtained via single point DFT calculations, performed with the program package ORCA (v 2.9.1)[52] with the B3LYP functional in combination with the EPRII basis set.[53-54] For non-polar solvents such as toluene, which was used for the EPR samples, solvation models such as COSMO have not generally improved the agreement between calculations and experiments[31] and were not used here. To test the influence of the basis set on the calculated EPR parameters, additional single point calculations using the same geometry (optimized at 6-31G+(d) basis containing both diffuse and polarized terms) and the def2-TZVPP basis set of Ahlrich's and co-workers[55-57] were performed and compared to the EPRII results. The principal g-values were calculated employing the coupled-perturbed Kohn-Sham equations and the spin orbit operator computed using the RI approximation for the Coulombic term and the one-center approximation for the exchange term (RIJCOSX SOMF(1X)).[58] The anisotropic magnetic dipole and the isotropic Fermi contact contributions to the hyperfine coupling were calculated for all ^{1}H and ^{13}C atoms. To determine the effect of the basis set used in optimization, all structures were optimized *in vacuo* using 3-21G, 6-31G, and 6-31G+(d) basis sets, using

successively, the 3-21G, 6-31G, and the 6-31G+(d) basis sets. In general, increasing the basis set had little effect on the structure with RMSD values for the fullerene itself around 0.01 Å between the 6-31G and the 6-31+G(d) and around 0.1 Å between the 3-21G and the 6-31G+(d) basis sets. Calculation of the EPR g-values for each structure gave very similar results (SI Table S1). Furthermore, the EPR parameters calculated using the EPRII basis set are very similar to those calculated using the larger def2-TZVPP basis set (SI Table S2). Finally, to assess the robustness of the results with respect to functional choice, the g-values were calculated using a variety of functionals (SI Table S3). Atomic coordinates for all structures at the 6-31G+(d) level are given in the supporting information (SI Tables S3-S6).

ASSOCIATED CONTENT

Supporting Information Available: Comparison of structures and EPR parameters calculated using various functionals and basis sets, selected bonds lengths, atomic coordinates, spin populations and hyperfine coupling constants for selected structures, spin density plots for selected cases. This material is available free of charge via the Internet at http://pubs.acs.org.

AUTHOR INFORMATION

Corresponding Author

*Email: kmardis@csu.edu; oleg@anl.gov

Notes

The authors declare no competing financial interests.

ACKNOWLEDGMENTS

This material is based upon work supported by U.S. Department of Energy, Office of Science, Office of Basic Energy Sciences, Division of Chemical Sciences, Geosciences, and Biosciences, under contract number DE-AC02-06CH11357 at Argonne National Laboratory (JN and OPG). KLM was supported by the Illinois Space Grant Consortium. JNW was supported by the NIH/NIGMS (R25 GM059218) and TH was supported by the Army Research Laboratory (Contract W911NF-08-20039).

REFERENCES

(1) Snow, N. Exxon Mobil Forecasts 35% Higher World Energy Demand by 2040. *OGJ* **2014,** *12b*, 22.
(2) Cho, A. Energy's Tricky Tradeoffs. *Science* **2010,** *329*, 786-787.
(3) Chu, S.; Majumdar, A. Opportunities and Challenges for a Sustainable Energy Future. *Nature* **2012,** *488*, 294-303.
(4) Lewis, N. S.; Nocera, D. G. Powering the Planet: Chemical Challenges in Solar Energy Utilization. *Proc. Natl. Acad. Sci. U.S.A.* **2006,** *103*, 15729-15735.
(5) Lewis, N. S. Toward cost-effective Solar Energy Use. *Science* **2007,** *315*, 798-801.
(6) Cook, T. R.; Dogutan, D. K.; Reece, S. Y.; Surendranath, Y.; Teets, T. S.; Nocera, D. G. Solar Energy Supply and Storage for the Legacy and Non legacy Worlds. *Chem. Rev.* **2010,** *110*, 6474-6502.
(7) Blankenship, R. E.; Tiede, D. M.; Barber, J.; Brudvig, G. W.; Fleming, G.; Ghirardi, M.; Gunner, M. R.; Junge, W.; Kramer, D. M.; Melis, A.*, et al.* Comparing Photosynthetic and Photovoltaic Efficiencies and Recognizing the Potential for Improvement. *Science* **2011,** *332*, 805-809.
(8) Brabec, C. J.; Gowrisanker, S.; Halls, J. J. M.; Laird, D.; Jia, S. J.; Williams, S. P. Polymer-Fullerene Bulk-Heterojunction Solar Cells. *Adv. Mater.* **2010,** *22*, 3839-3856.
(9) Green, M. A.; Ho-Baillie, A.; Snaith, H. J. The emergence of perovskite solar cells. *Nature Photon.* **2014,** *8*, 506-514.
(10) Kazim, S.; Nazeeruddin, M. K.; Gratzel, M.; Ahmad, S. Perovskite as Light Harvester: A Game Changer in Photovoltaics. *Angew. Chem. Int. Ed.* **2014,** *53*, 2812-2824.
(11) Grätzel, M. Recent Advances in Sensitized Mesoscopic Solar Cells. *Acc. Chem. Res.* **2009,** *42*, 1788-1798.
(12) Green, M. A. *Third Generation Photovoltaics: Advanced Solar Energy Conversion*; Springer: Berlin; 2005.
(13) Sariciftci, N. S.; Smilowitz, L.; Heeger, A. J.; Wudl, F. Photoinduced Electron-Transfer from a Conducting Polymer to Buckminsterfullerene. *Science* **1992,** *258*, 1474-1476.

(14) Green, M. A.; Emery, K.; Hishikawa, Y.; Warta, W.; Dunlop, E. D. Solar cell efficiency tables (version 46). *Prog. Photovoltaics* **2015,** *23*, 805-812.
(15) Khlyabich, P. P.; Burkhart, B.; Rudenko, A. E.; Thompson, B. C. Optimization and Simplification of Polymer-Fullerene Solar Cells through Polymer and Active Layer Design. *Polymer* **2013,** *54*, 5267-5298.
(16) Deibel, C.; Dyakonov, V. Polymer-Fullerene Bulk Heterojunction Solar Cells. *Rep. Prog. Phys.* **2010,** *73*, 096401.
(17) Boudreault, P. L. T.; Najari, A.; Leclerc, M. Processable Low-Bandgap Polymers for Photovoltaic Applications. *Chem. Mat.* **2011,** *23*, 456-469.
(18) Liang, Y. Y.; Yu, L. P. A New Class of Semiconducting Polymers for Bulk Heterojunction Solar Cells with Exceptionally High Performance. *Acc. Chem. Res.* **2010,** *43*, 1227-1236.
(19) Clarke, T. M.; Durrant, J. R. Charge Photogeneration in Organic Solar Cells. *Chem. Rev.* **2010,** *110*, 6736-6767.
(20) Hummelen, J. C.; Knight, B. W.; Lepeq, F.; Wudl, F.; Yao, J.; Wilkins, C. L. Preparation and Characterization of Fulleroid and Methanofullerene Derivatives. *J. Org. Chem.* **1995,** *60*, 532-538.
(21) Wienk, M. M.; Kroon, J. M.; Verhees, W. J. H.; Knol, J.; Hummelen, J. C.; van Hal, P. A.; Janssen, R. A. J. Efficient methano[70]fullerene/MDMO-PPV Bulk Heterojunction Photovoltaic Cells. *Angew. Chem. Int. Ed.* **2003,** *42*, 3371-3375.
(22) Bennebroek, M. T.; Arnold, A.; Poluektov, O. G.; Baranov, P. G.; Schmidt, J. Shallow electron centers in silver halides. *Phys. Rev. B* **1996,** *54*, 11276-11289.
(23) Baranov, P. G.; Romanov, N. G.; Poluektov, O. G.; Schmidt, J. Self-Trapped Excitons in Ionic-Covalent Silver Halide Crystals and Nanostructures: High-Frequency EPR, ESE, ENDOR and ODMR Studies. *Appl. Magn. Reson.* **2010,** *39*, 453-486.
(24) Matsumoto, T.; Poluektov, O. G.; Schmidt, J.; Mokhov, E. N.; Baranov, P. G. Electronic Structure of the Shallow Boron Acceptor in 6H-SiC: A Pulsed EPR/ENDOR Study at 95 GHz. *Phys. Rev. B* **1997,** *55*, 2219-2229.
(25) Carrington, A.; McLachlan, A. D. *Introduction to Magnetic Resonance*; Harper & Row: New York; 1969.
(26) Weil, J. A.; Bolton, J. R.; Weil, J. A.; Bolton, J. R.; Wertz, J. E. *Electron Paramagnetic Resonance: Elementary Theory and Practical Applications*; John Wiley & Sons: New York; 2007.
(27) Gordy, W. *Theory and Applications of Electron Spin Resonance*; John Wiley & Sons: New York; 1980.
(28) Poluektov, O. G.; Filippone, S.; Martin, N.; Sperlich, A.; Deibel, C.; Dyakonov, V. Spin Signatures of Photogenerated Radical Anions in Polymer-[70]Fullerene Bulk Heterojunctions: High Frequency Pulsed EPR Spectroscopy. *J. Phys. Chem. B* **2010,** *114*, 14426-14429.
(29) Liedtke, M.; Sperlich, A.; Kraus, H.; Deibel, C.; Dyakonov, V.; Filippone, S.; Delgado, J. L.; Martín, N.; Poluektov, O. G. Spectroscopic Signatures of Photogenerated Radical Anions in Polymer-[C_{70}]Fullerene Bulk Heterojunctions. *ECS Trans.* **2010,** *28*, 3-10.
(30) De Ceuster, J.; Goovaerts, E.; Bouwen, A.; Hummelen, J. C.; Dyakonov, V. High-frequency (95 GHz) Electron Paramagnetic Resonance Study of the Photoinduced Charge Transfer in conjugated Polymer-Fullerene Composites. *Phys. Rev. B* **2001,** *64*, 195206.
(31) Niklas, J.; Mardis, K. L.; Banks, B. P.; Grooms, G. M.; Sperlich, A.; Dyakonov, V.; Beaupre, S.; Leclerc, M.; Xu, T.; Yu, L.*, et al.* Highly-Efficient Charge Separation and Polaron

Delocalization in Polymer-Fullerene Bulk-Heterojunctions: A Comparative Multi-Frequency EPR and DFT Study. *Phys. Chem. Chem. Phys.* **2013,** *15*, 9562-9574
(32) Adrian, F. J. Spin-Orbit Effects in Fullerenes. *Chem. Phys.* **1996,** *211*, 73-80.
(33) Dubois, D.; Kadish, K. M.; Flanagan, S.; Haufler, R. E.; Chibante, L. P. F.; Wilson, L. J. Spectroelectrochemical Study of the C_{60} and C_{70} Fullerenes and their Mono-, Di-, Tri-, and Tetraanions. *J. Am. Chem. Soc.* **1991,** *113*, 4364-4366.
(34) Poluektov, O. G.; Niklas, J.; Mardis, K. L.; Beaupre, S.; Leclerc, M.; Villegas, C.; Erten-Ela, S.; Delgado, J. L.; Martin, N.; Sperlich, A.*, et al.* Electronic Structure of Fullerene Heterodimer in Bulk-Heterojunction Blends. *Adv. Energy Mater.* **2014**, 1301517.
(35) Niklas, J.; Holt, J. M.; Mistry, K.; Rumbles, G.; Blackburn, J. L.; Poluektov, O. G. Charge Separation in P3HT:SWCNT Blends Studied by EPR: Spin Signature of the Photoinduced Charged State in SWCNT. *J. Phys. Chem. Lett.* **2014,** *5*, 601-606.
(36) Niklas, J.; Beaupre, S.; Leclerc, M.; Xu, T.; Yu, L. P.; Sperlich, A.; Dyakonov, V.; Poluektov, O. G. Photoinduced Dynamics of Charge Separation: From Photosynthesis to Polymer-Fullerene Bulk Heterojunctions. *J. Phys. Chem. B* **2015,** *119*, 7407-7416.
(37) Smirnova, T. I.; Chadwick, T. G.; Voinov, M. A.; Poluektov, O.; van Tol, J.; Ozarowski, A.; Schaaf, G.; Ryan, M. M.; Bankaitis, V. A. Local Polarity and Hydrogen Bonding Inside the Sec14p Phospholipid-Binding Cavity: High-field Multi-Frequency Electron Paramagnetic Resonance Studies. *Biophys. J.* **2007,** *92*, 3686-3695.
(38) Owenius, R.; Engstrom, M.; Lindgren, M.; Huber, M. Influence of Solvent Polarity and Hydrogen Bonding on the EPR Parameters of a Nitroxide Spin Label Studied by 9-GHz and 95-GHz EPR Spectroscopy and DFT calculations. *J. Phys. Chem. A* **2001,** *105*, 10967-10977.
(39) Plato, M.; Steinhoff, H. J.; Wegener, C.; Torring, J. T.; Savitsky, A.; Möbius, K. Molecular Orbital Study of Polarity and Hydrogen Bonding Effects on the g and Hyperfine Tensors of Site Directed NO Spin Labelled Bacteriorhodopsin. *Mol. Phys.* **2002,** *100*, 3711-3721.
(40) Powell, W. H.; Cozzi, F.; Moss, G. P.; Thilgen, C.; Hwu, R. J. R.; Yerin, A. Nomenclature for the C_{60}-I_h and C_{70}-$D_{5h(6)}$ Fullerenes - (IUPAC recommendations 2002). *Pure Appl. Chem.* **2002,** *74*, 629-695.
(41) Filatov, M.; Cremer, D. Calculation of Spin-Densities within the Context of Density Functional Theory. The Crucial Role of the Correlation Functional. *J. Chem. Phys* **2005,** *123*, 7.
(42) Bresgunov, A. Y.; Dubinskii, A. A.; Krimov, V. N.; Petrov, Y. G.; Poluektov, O. G.; Lebedev, Y. S. Pulsed EPR in 2-mm Band. *Appl. Magn. Reson.* **1991,** *2*, 715-728.
(43) Poluektov, O. G.; Utschig, L. M.; Schlesselman, S. L.; Lakshmi, K. V.; Brudvig, G. W.; Kothe, G.; Thurnauer, M. C. Electronic Structure of the P_{700} Special Pair from High-Frequency Electron Paramagnetic Resonance Spectroscopy. *J. Phys. Chem. B* **2002,** *106*, 8911-8916.
(44) Stoll, S.; Schweiger, A. EasySpin, a Comprehensive Software Package for Spectral Simulation and Analysis in EPR. *J. Magn. Reson.* **2006,** *178*, 42-55.
(45) PDB starting structure available upon request.
(46) Salonen, E.; Lin, S.; Reid, M. L.; Allegood, M.; Wang, X.; Rao, A. M.; Vattulainen, I.; Ke, P. C. Real-Time Translocation of Fullerene Reveals Cell Contraction. *Small* **2008,** *4*, 1986-1992.
(47) Becke, A. D. Density-Functional Thermochemistry .3. The Role of Exact Exchange. *J. Chem. Phys* **1993,** *98*, 5648-5652.

(48) Stephens, P. J.; Devlin, F. J.; Chabalowski, C. F.; Frisch, M. J. Ab-Initio Calculation of Vibrational Absorption and Circular-Dichroism Spectra Using Density-Functional Force-Fields. *J. Phys. Chem.* **1994,** *98*, 11623-11627.
(49) Lee, C. T.; Yang, W. T.; Parr, R. G. Development of the Colle-Salvetti Correlation-Energy Formula into a Functional of the Electron-Density. *Phys. Rev. B* **1988,** *37*, 785-789.
(50) Vosko, S. H.; Wilk, L.; Nusair, M. Accurate Spin-Dependent Electron Liquid Correlation Energies for Local Spin-Density Calculations - a Critical Analysis. *Can. J. Phys.* **1980,** *58*, 1200-1211.
(51) Baker, J.; Wolinski, K.; Malagoli, M.; Kinghorn, D.; Wolinski, P.; Magyarfalvi, G.; Saebo, S.; Janowski, T.; Pulay, P. Quantum Chemistry in Parallel with PQS. *J. Comput. Chem.* **2009,** *30*, 317-335.
(52) Neese, F. The ORCA Program System. *WIREs Comput. Mol. Sci.* **2012,** *2*, 73-78.
(53) Rega, N.; Cossi, M.; Barone, V. Development and Validation of Reliable Quantum Mechanical Approaches for the Study of Free Radicals in Solution. *J. Chem. Phys* **1996,** *105*, 11060-11067.
(54) Barone, V. Structure, Magnetic Properties and Reactivities of Open-Shell Species from Density Functional and Self-Consistent Hybrid Methods. In *Recent Advances in Density Functional Methods (Part 1)*, Chong, D. P., Ed., World Scientific: Singapore, 1995; pp 287-334.
(55) Weigend, F.; Ahlrichs, R. Balanced Basis Sets of Split Valence, Triple Zeta Valence and Quadruple Zeta Valence Quality for H to Rn: Design and Assessment of Accuracy. *Phys. Chem. Chem. Phys.* **2005,** *7*, 3297-3305.
(56) Schäfer, A.; Huber, C.; Ahlrichs, R. Fully Optimized Contracted Gaussian-Basis Sets of Triple Zeta Valence Quality for Atoms Li to Kr. *J. Chem. Phys* **1994,** *100*, 5829-5835.
(57) Schäfer, A.; Horn, H.; Ahlrichs, R. Fully Optimized Contracted Gaussian-Basis Sets for Atoms Li to Kr. *J. Chem. Phys* **1992,** *97*, 2571-2577.
(58) Neese, F. Efficient and Accurate Approximations to the Molecular Spin-Orbit Coupling Operator and their Use in Molecular g-Tensor Calculations. *J. Chem. Phys* **2005,** *122*, 034107.